Time reversed imaging as a diagnostic of wave and particle chaos

R.K. Snieder(2,3) and J.A. Scales(1,2)

(1) Department of Geophysics and (2) Center for Wave Phenomena,
Colorado School of Mines,
Golden CO 80401, USA

(3) Dept. of Geophysics,
Utrecht University, P.O. Box 80.021,
3508 TA Utrecht, Netherlands

July 1, 1998

Heading: In the presence of multiple scattering, waves and particles behave fundamentally differently. As a model for the stability of the temporal evolution of particle and wave propagation, a scattering system is presented in which particle propagation is strongly unstable while wave propagation is significantly more stable. Both analytical and numerical evidence for the different stability properties of wave and particle propagation is presented; the exponential divergence of particle trajectories leads to a critical length scale for the stability of particle propagation that depends exponentially on time ($\exp(-\mu t)$), whereas the critical length scale for the stability of wave propagation decreases with time only as $1/\sqrt{t}$. This fundamental difference is due to wave suppression of classical chaos that is intimately related to the concept of ray splitting.

1 Time-reversed-imaging as a diagnostic

The relation of classical chaotic motion and the corresponding behavior of waves that propagate in the same system has been an active field of research. The words "quantum chaos" suggest that quantum systems can exhibit chaotic behavior. Classical chaotic systems display a fractal structure in phase space. Such a fractal structure in phase space is precluded

in quantum mechanics by Heisenberg's uncertainty principle. In addition, closed quantum system have discrete states that correspond to periodic motion, whereas classical chaos is characterized in the frequency domain by a continuous spectrum [1]. It is thus not clear what the imprint of chaos on quantum-mechanical systems is. For this reason Berry [2] introduced the phrase "quantum chaology." The relation between classical chaos and quantum chaos is not trivial [3]. For classical systems the KAM-tori form impenetrable barriers, but waves can tunnel through these barriers. Conversely, cantori (broken up KAM-tori) can be penetrated by classical trajectories but the finite extent of a wave in phase space practically blocks the waves from crossing a cantorus. In addition, classical trajectories that nearly touch each other are fundamentally different from a classical point of view, but for the corresponding quantum system these touching trajectories lead to new phenomena [4].

Although many aspects of the relation between classical chaos and quantum chaos are not completely understood it is clear that wave effects suppress the chaotic character of systems; one can speak of a quantum suppression of classical chaos [3]. This notion has been formulated in the following way by Gutzwiller [5]:

> "Quantum mechanics mitigates the destructive influence of classical chaos on simple physical processes. Indeed, quantum mechanics is sorely needed to save us from the bizarre aspects of classical mechanics; but most paradoxically this process of softening the many rough spots is entirely in our grasp as soon as the nature of the roughness is understood."

It is the goal of this work to obtain a better understanding of the imprint of classical chaos on wave systems.

The stability of wave and particle propagation is studied here using time-reversed-imaging (TRI). The concept of TRI relies on the invariance of Newton's law or the wave equation under time-reversal. Consider a wave or particle system that evolves forward in time from a source at time $t = 0$ to a later time t. When the motion of the particles or the wave vector of the waves are reversed at this time, the particles and waves will retrace their original trajectories and return to the source where they originally started. However, when the system is perturbed before the reverse propagation the particles or waves do not necessarily return to their original source. The inability to return to the original source position is related to the stability of the wave or

particle propagation to perturbations. Ballentine and Zibin [6] used reverse time propagation to study the stability of wave and particle propagation for the driven quartic oscillator and the periodically kicked rotator when the systems were perturbed by a uniform translation.

This study has been driven by recent laboratory experiments of TRI of acoustic and elastic waves ([7], [8], [9]). In these experiments TRI is achieved by driving one or more piezoelectric transducers with a time-reversed version of the recorded wave field. The process has proven to be surprisingly stable, even for an experiment involving a medium with 2000 strong scatterers [7]. In [9] the ergodicity of stadium boundaries has been exploited to achieve TRI of elastic waves experimentally with only a *single* receiver.

The degree of focusing of waves under TRI depends on the aperture of the receiver array, the initial errors in the reversed wave field and on the stability properties of wave propagation. For closed systems of particles with perfectly reflecting walls (i.e., billiards), certain boundary geometries are known to be ergodic (e.g., [10]). This ergodicity, combined with a sensitive dependence on initial conditions is the definition of chaos [1]. For open systems of particles and for waves the situation is less clear. TRI provides a diagnostic of the stability of propagation that can be used for both particles and waves in open or closed systems. The idea is that for a system that is time-reversal invariant, both particles and waves should return to their source when at a certain time the waves and particles are reversed. A complete focusing on the source will only take place when the velocity and position are known exactly and when the scattering medium is exactly the same before and after the time reversal. The degree to which errors in these quantities destroy the imaging on the source is a diagnostic of the stability of the wave or particle propagation, and hence of chaotic behavior of particles and waves.

In [11] we show that the delicate interference required to achieve TRI of waves can be destroyed by relatively small perturbations in the position of the scatterers. Here we address systematically the stability of TRI under various kinds of perturbations for open systems of both particles and waves in the presence of multiple scattering. The system used here is similar to the one used in [7] and is shown in Fig. 1. Particles or waves are emitted from a source and propagate through a system of 200 strong isotropic point scatterers. For the waves, 96 receivers are located on the line indicated in Fig. 1. A particle is recorded for the time-reversed imaging when it traverses the receiver line.

When comparing the stability of wave or particle propagation, one can either specify the medium (e.g. a quantum mechanical potential) or the scat-

tering properties of the waves and particles. When the medium is fixed, the relation between the wave system and the classical system can be obtained by letting the wavelength approach zero ($\lambda \rightarrow 0$), or equivalently in the case of quantum mechanics letting Planck's constant go to zero ($\hbar \rightarrow 0$). This limit can be studied using semiclassical mechanics [5][12], this can even be achieved for wave systems that exhibit ray-splitting [13][14]. In this work the scattering properties of the waves and the particles are taken to be identical by using isotropic point scatterers with the same scattering cross section for both waves and particles. This choice ensures that the only difference between the waves and particles lies in the dynamics of propagation, rather than in a different interaction with the scatterers.

2 Scattering of particles

Isotropic scattering of particles that is invariant under time reversal is ensured by requiring that both the velocity v ($=1500\ m/s$) and the impact parameter b of the particles are conserved during scattering and that (in two dimensions) the scattering angle Θ is linear in the impact parameter:

$$\Theta = \pi \left(\frac{\sigma - 2b}{\sigma} \right) \qquad for \quad |b| \leq \sigma/2 \ , \tag{1}$$

where σ is the scattering cross-section. For larger values of the impact parameter the particle is not scattered (i.e. $\Theta = 0$). The impact parameter is defined geometrically in Fig. 2. See Table 1 for the values of parameters in the numerical experiment. Figure 3 shows the mean number of encounters n with scatterers for the particles that cross the receiver line as a function of time t. To a very good approximation the number of scatterers encountered increases linearly with time:

$$n = vt/l \ , \tag{2}$$

where t is the time relative to the arrival time of the direct transmitted wave. A least-squares fit of the line in Fig. 3 gives the value of the mean free path: $l = 15.56mm$. This quantity is much less than the size of the scattering region ($80mm$), which implies that the particles are strongly scattered. For the TRI of the particles, the velocity of the particles is reversed when they cross the receiver line and t is replaced by $-t$; in ideal circumstances the particle should then return to the source at $t = 0$.

3 Scattering of waves

Consider a model of isotropic point scatterers at location $\mathbf{r}_j$. The complex scattering coefficient of scatterer j is denoted by A_j. This coefficient contains the full nonlinear interaction of the wave that is incident on the scatterer and the scattered wave. Let the total wave field that is incident on scatterer j be denoted by u_j. The wave that is scattered by this scatterer is then given by $G(\mathbf{r}, \mathbf{r}_j) A_j u_j$, where $G(\mathbf{r}, \mathbf{r}')$ is the Green's function of the medium in which the scatterers are embedded. Since the scattering is assumed to be isotropic, there is no dependence on the scattering angle. The total wave field can be written as the superposition of the unperturbed wave $u^{(0)}(\mathbf{r})$ and the waves emanating from all the scatterers:

$$u(\mathbf{r}) = u^{(0)}(\mathbf{r}) + \sum_j G(\mathbf{r}, \mathbf{r}_j) A_j u_j \ . \tag{3}$$

The wave field that is incident on scatterer i follows from this expression by setting $\mathbf{r} = \mathbf{r}_i$, and by omitting the term $j = i$ from the sum in (3) because the wave incident wave on scatterer i only has contributions from the unperturbed wave and from the waves coming from the other scatterers:

$$u_i = u_i^{(0)} + \sum_{j \neq i} G(\mathbf{r}_i, \mathbf{r}_j) A_j u_j \ , \tag{4}$$

where $u_i^{(0)}$ is the unperturbed wave at each scatterer: $u_i^{(0)} = u^{(0)}(\mathbf{r}_i)$. Equation (4) constitutes a linear system of equations for the complex coefficients u_j. This system can be solved numerically. Once the u_j are determined one can compute the wave field at any location $\mathbf{r}$ by inserting the u_j in expression (3). Equations (3) and (4) give the exact response of a system of isotropic point scatterers and allows us to use the same scattering cross-section for the waves and the particles. Examples of the wave field computed with this method are given in [15].

For convenience the equations (4) can also be written in vector form:

$$(\mathbf{I} - \mathbf{S})\, \mathbf{u} = \mathbf{u}^{(0)} \ , \tag{5}$$

where $\mathbf{u}$ is the vector with u_j as the j-th component and $\mathbf{u}^{(0)}$ has $u^{(0)}(\mathbf{r}_j)$ as the j-th component. $\mathbf{I}$ is the identity matrix and the components of the matrix $\mathbf{S}$ are given by:

$$S_{ij} = \begin{cases} 0 & for\ i = j \\ G(\mathbf{r}_i, \mathbf{r}_j) A_j & for\ i \neq j \end{cases} \tag{6}$$

For elastic scatterers, the optical theorem[16][17] imposes a constraint on the imaginary component of the forward scattering amplitude and the scattered power averaged over all directions. For isotropic point scatterers the optical theorem imposes the following constraint on the scattering coefficient in different dimensions:

$$\Im m(A) = \begin{cases} -\frac{1}{2k}\left|A\right|^2 & in\ 1D \\ -\frac{1}{4}\left|A\right|^2 & in\ 2D \\ -\frac{k}{4\pi}\left|A\right|^2 & in\ 3D \end{cases} \tag{7}$$

Note that the scattering formalism can be applied to any number of dimensions and that the numerical implementation is very similar in different number of dimensions.

The scattering equations (3) and (4) can be rewritten in a different form that is useful for a number of applications. The linear system of equations (5) can be solved by matrix inversion: $\mathbf{u} = (\mathbf{I} - \mathbf{S})^{-1}\,\mathbf{u}^{(0)}$. Using an expansion of the inverse $(\mathbf{I} - \mathbf{S})^{-1}$ this can also be written as:

$$\mathbf{u} = \mathbf{u}^{(0)} + \mathbf{S}\mathbf{u}^{(0)} + \mathbf{S}^2\mathbf{u}^{(0)} + \mathbf{S}^3\mathbf{u}^{(0)} + \cdots \tag{8}$$

Inserting this expression in (3) and using the definition (6) for $\mathbf{S}$, the total wave field is given by

$$u(\mathbf{r}) = u^{(0)}(\mathbf{r}) + \sum_i G(\mathbf{r},\mathbf{r}_i)A_i u^{(0)}(\mathbf{r}_i) + \sum_{i\neq j}\sum_j G(\mathbf{r},\mathbf{r}_i)A_i G(\mathbf{r}_i,\mathbf{r}_j)A_j u_j + \ldots \tag{9}$$

This result can be seen as the Neumann series solution of the scattering problem. The series does have a clear physical meaning because it is a sum over all possible paths joining scatterers with the provision that the same scatterer is not included on consecutive scattering events:

$$u(\mathbf{r}) = \sum_P e^{ikL_P}\left(\prod C\right)u^0\ . \tag{10}$$

In this expression L_P is the path length of the path ending at location $\mathbf{r}$ and u^0 is the source signal emitted from the sources and $\prod C$ gives the product of geometrical spreading and scattering coefficients for the paths between scatterers. In case multiple sources are present a summation over these sources is implied. The significance of this expression is that the total wave-field is written as a sum over all possible paths joining the scatterers, in this way it constitutes a discrete version of the Feynman path integral.

TRI of the waves is carried out by recording the wave-field at 96 equidistant receivers on the receiver line, and by using the complex conjugate of the wave-field in the frequency domain as source signals that are emitted from the receivers. The wave field recorded at the middle receiver is shown in Fig. 4. Note that the wave-field is characterized by a slowly decaying wave train of scattered waves. This reflects the fact that for the employed parameter setting strong multiple scattering occurs.

4 Stability analysis for scattered particles

Consider a particle that is scattered once with impact parameter b and with a perturbed impact parameter $b+\Delta$. Using (1) the divergence of the trajectories is given by $|\mathbf{r}_{b+\Delta}(t) - \mathbf{r}_b(t)| \approx vt\,(\Theta(b+\Delta) - \Theta(b)) = 2\pi vt\Delta/\sigma$. This implies that the error Δ_{out} at time t since the scattering is related to the initial error Δ_{in} by $\Delta_{out} = 2\pi\,(vt/\sigma)\,\Delta_{in}$. On average, vt is the mean-free path l, hence

$$\Delta_{out} = 2\pi\,(l/\sigma)\,\Delta_{in}\ . \tag{11}$$

When a particle is scattered n times, the error Δ_n follows by recursion:

$$\Delta_n = (2\pi l/\sigma)^n\,\Delta_0\ . \tag{12}$$

The number of scatterer encounters is on average given by $n = vt/l$, hence the Lyapunov exponent μ associated with the exponential divergence of trajectories is given by

$$\mu = \ln\,(2\pi l/\sigma)\ \ v/l\ . \tag{13}$$

Equation (12) gives the error in the trajectory after n scattering encounters. The error δ in the TRI is given by $\delta = D\,(\Delta\Theta) = D(d\Theta/db)\Delta_n$, hence

$$\delta = \frac{2\pi D}{\sigma}\left(\frac{2\pi l}{\sigma}\right)^n\,\Delta_0\ , \tag{14}$$

where D is the distance from the scattering region to the source position, see Fig. 1. When the error in the trajectory is of the order of $\sigma/2$, the trajectory will be completely different because the particle then encounters different scatterers. The associated critical perturbation δ_c follows from (12):

$$\delta_c = \left(\frac{\sigma}{2\pi l}\right)^n\,\frac{\sigma}{2}\ . \tag{15}$$

Using expression (13) for the Lyapunov exponent and using (2) to eliminate n one finds that this critical length scale decreases exponentially with time:

$$\delta_c = \frac{\sigma}{2}\, e^{-\mu t} \ . \tag{16}$$

For the numerical experiments the critical length scale is shown in Table 2 as a function of the number of encountered scatterers. Also indicated is the precision with which the numerical simulations have been carried out. (All calculations were done in 64 bit arithmetic on an SGI Power Challenge.) Since the mean free path l is much larger than the scattering cross-section σ (Table 1) the critical length scale decreases dramatically with the number of scattering encounters.

The previous analysis applies for a perturbation of the starting point of a particle. When the scatterer locations are perturbed over a distance δ, a term δ should be added to the right-hand side of (11). The error after n scattering encounters is then given by

$$\Delta_n = \left(\frac{\left(\frac{2\pi l}{\sigma}\right)^{n+1} - 1}{\left(\frac{2\pi l}{\sigma}\right) - 1} \right) \Delta_0 \ . \tag{17}$$

However, given the high numerical value of $2\pi l/\sigma$ (≈ 61) in the numerical experiments this result is similar to (12) for the perturbation of initial conditions. The associated critical length scale is shown in Table 3.

It follows that for the particles the critical length scale depends on the scattering cross section and the mean free path, and that this quantity decreases exponentially with the number of scattering encounters (and thus decreases exponentially with time). Due to this dependence the critical length scale δ_c is dramatically smaller than the scattering cross section σ.

5 Stability analysis for scattered waves

A fundamental difference between time reversed imaging of waves and particles is that TRI of particles occurs because a trajectory returns to the source at $t = 0$ whereas for waves TRI is achieved because the waves interfere at $t = 0$ constructively only near the source. When either the sources or the scatterers are perturbed for the waves, the dominant effect on the wave-field is the perturbation of the path lengths L_P in (10). When the variance σ_L of the path length is of the order of a quarter wavelength (denoted by λ) the

resulting interference pattern is destroyed. Hence TRI of waves will break down when $\sigma_L \approx \lambda/4$. This implies that the decoherence of the interfering multiple scattered waves leads to the irreversibility of the wave field [18].

The effect of the perturbation in the i-th component of the position vector of scatterer j on the path length L_P follows from the derivative

$$\frac{\partial L_P}{\partial x_i^{(j)}} = \frac{x_i^{(j)} - x_i^{(j-1)}}{\left|\mathbf{r}^{(j)} - \mathbf{r}^{(j-1)}\right|} - \frac{x_i^{(j+1)} - x_i^{(j)}}{\left|\mathbf{r}^{(j+1)} - \mathbf{r}^{(j)}\right|} , \tag{18}$$

which implies that

$$\sum_i \left(\frac{\partial L_P}{\partial x_i^{(j)}} \right)^2 = 2 - 2 \frac{\left(\mathbf{r}^{(j)} - \mathbf{r}^{(j-1)}\right) \cdot \left(\mathbf{r}^{(j+1)} - \mathbf{r}^{(j)}\right)}{\left|\mathbf{r}^{(j)} - \mathbf{r}^{(j-1)}\right| \left|\mathbf{r}^{(j+1)} - \mathbf{r}^{(j)}\right|} = 2 \left(1 - \cos \Theta_j\right) , \tag{19}$$

where Θ_j is the scattering angle at scatterer j. This angle is related to the angle φ_j in Fig. 9 by the relation $\Theta_j = \varphi_j - \varphi_{j-1}$. When the perturbations of the locations of different scatterers are independent, the total variance in the path length is thus given by

$$\sigma_L^2 = \sum_j 2 \left(1 - \cos \Theta_j\right) \delta^2 . \tag{20}$$

For the coda (the later part of the wave field consisting of multiply-scattered waves) the cosine of the scattering angle has zero mean because all scattering angles are equally likely: $\langle \cos \Theta_j \rangle = 0$. Using this, it follows from (20) that the variance in the path length joining n scatterers is given by

$$\sigma_L^{coda} = \sqrt{2n}\ \delta . \tag{21}$$

TRI of the coda breaks down when this quantity equals $\lambda/4$. The critical length scale for perturbations of the scatterer locations is thus given by

$$\delta_c^{coda} = \lambda / \left(4\sqrt{2n}\right) , \tag{22}$$

see Table 3. Note that in contrast to the situation for particles this critical length scale does not depend exponentially on n. Using the fact that the number of encountered scatterers increases linearly with time (2) one finds that the critical length scale for the coda waves varies with time as $\delta_c^{coda} \sim 1/\sqrt{t}$. This time-dependence of the critical length scale for the coda waves is in stark contrast with the exponential decrease of the critical length scale

for the particles with time given in (16). The $1/\sqrt{t}$ time-dependence of the critical length scale was also obtained by Ballentine and Zibin [6] who show that for a periodically kicked rotator with a kick-strength that leads to classical solutions that are chaotic, the critical rotation angle $\delta\theta_{1/2}$ varies with time as $1/\sqrt{t}$ for large time.

For the ballistic wave (the wave that propagates along the line of sight from source to receiver) only forward scattering is of relevance. For forward scattering the term $(1 - \cos\Theta_j) \approx \Theta_j^2/2$ is small because the scattering angle is small. This leads to a reduction of the variance with a factor λ/L. The detailed analysis in appendix A shows that

$$\sigma_L^{ball} \approx \sqrt{\frac{3(n+1)}{4}} \sqrt{\frac{\lambda}{L}}\, \delta \ . \tag{23}$$

When σ_L^{ball} is about a quarter wavelength the interference is upset, hence the critical length scale is given by

$$\delta_c^{ball} \approx \sqrt{\lambda L}/\sqrt{12(n+1)} \ , \tag{24}$$

(see Table 3). Note that this length scale is proportional to the width $\sqrt{\lambda L}$ of the first Fresnel zone; when a scatterer is moved over the width of the Fresnel zone it contributes in a fundamentally different way to the ballistic wave.

When the source locations are perturbed over a distance δ but the scatterers remain fixed, only the length of the trajectory to the first scatterer is perturbed. This means that for this perturbation for both the coda and the ballistic wave $\sigma_L = \delta$. Thus, the critical length scale for perturbation of the source locations for both the coda and the ballistic wave is given by $\delta_c^{source} = \lambda/4$, see Table 3.

6 Numerical simulations

In the TRI of particles 20,000 particles are propagated from the source to the receiver line and after time-reversal back-propagated to the source. For the case when the receivers and the scatterers are not perturbed, the only relevant error is the finite precision arithmetic in the numerical calculations. It follows from Table 2 that particles with more than 8 scattering encounters will not be focused on the source during TRI. The numerical experiments confirm this conclusion. Figure 5 shows the location of the particles after TRI

at $t = 0$ as a function of position. In the ideal case, all particles are imaged on the source at $x = z = 0$. For the particles with 6 or fewer scattering encounters (top panel) this is indeed the case, whereas the particles with 10 or more encounters (bottom panel) are imaged quasi-randomly over the whole region. The particles with 7-9 encounters (middle panel) are at $t = 0$ localized near the source region, but the imaging is degraded.

The quality of the time-reversed-image is quantified by $\exp(-error/D)$, where *error* denotes the mean distance of the particles to the source at $t = 0$. This imaging quality is shown in Fig. 6 as a function of the error in the source position for various values of the scattering encounter n. The critical length scale shown in Table 2 is indicated with the vertical arrows. The horizontal scale ends at the left with the machine precision. When the TRI degrades, the imaging quality decays from unity to zero, it follows from Fig. 6 that the analytical estimates of section agree well with the numerical results. When the scatterer locations are perturbed rather than the source locations, the results are virtually the same. This is due to the fact that for large values of $2\pi l/\sigma$ the expressions (12) and (17) are almost identical.

For the waves, TRI has been carried for several time windows, see Table 4. The imaged section along the line $z = 0$ of Fig. 1 is shown in Fig. 7 by the thick solid line. In this example, a short time window of the coda from 0.25 s to 0.30 ms has been used. The waves in this time window are located in the later part of the decaying wave train of multiple scattered waves, see Fig. 4. The energy is focused on the source location at $z = 0$, the nonvanishing energy at other locations is due to the finite aperture of the receiver array used in the TRI. This section compares favorably with the experimental results in [7]. The thin lines in Fig. 7 give the imaged section for various values of the perturbation in source position; the number indicates the variance in the perturbation of the source location measured in wavelengths. It can be seen that TRI indeed breaks down when the source locations are perturbed over about a quarter wavelength. The quality of the TRI can be quantified by computing the ratio of the amplitudes of the imaging peak of TRI with perturbation to the imaging peaks without perturbation.

The resulting relative peak heights are shown in Fig. 8 as a function of the error in source or scatterer locations for TRI experiments with the time windows shown in Table 4. The critical length scales shown in Table 3 are for each case indicated by vertical arrows. The curves for the perturbation of the source position are the four solid lines in the middle. These curves are identical for the four employed time windows and show a decay when the perturbation is of the order $\lambda/4$ (which has the numerical value 0.625

mm). For the perturbation of scatterers for TRI of the ballistic waves, the critical length scale is significantly larger, and agrees will with the critical length scale shown in Table 3. For TRI of the three coda intervals the critical length scale is appreciably less than a wavelength. The reason is that the number of scattering encounters is large for these waves (see Table 4). The agreement between numerical simulations and the estimates shown in Table 3 is very good. This confirms the assumption that the dominant effect of the perturbation of the time reversed imaging of waves is the perturbation of the path length.

7 Discussion

It follows from the TRI of particles and waves that the stability of particle and wave motion for the perturbation of initial conditions or scatterer locations is fundamentally different. In the numerical experiments particles that have encountered 8 or more scatterers do not return to the source after TRI, whereas waves that have encountered up to at least 30 scatterers (Table 4) focus well on the source after TRI. (With the employed numerical precision waves that have encountered significantly more scatterers can refocus on the source after TRI.) The physical reason for this difference is that particles follow a single trajectory. When the initial conditions or a scatterer along the trajectory are perturbed, the whole particle trajectory is perturbed, often in a dramatic fashion. Because of the chaotic nature of trajectories, the critical length scale is significantly less than the scattering cross-section by a factor that depends exponentially on the number of encountered scatterers and hence exponentially on time. This pertains both to the perturbation of the source position as well as to the perturbation of the scatterer position.

For the waves when the source or scatterer location is perturbed, the different wave-paths are not perturbed fundamentally; only the length of the wave-paths is changed. However, this perturbation only leads to appreciable effects when this perturbation is around a quarter-wavelength, because it is the interference of the waves along all possible wave-paths that determines the total wave-field. For both the coda and the ballistic wave the critical perturbation of the source location is a quarter-wavelength. For the perturbation of the scatterers the critical wavelength for the coda is proportional to the wavelength, but much smaller with a factor $1/\sqrt{2n}$. In contrast, the ballistic wave is only sensitive to perturbations of the scatterer position that are of the order of the width of the Fresnel zone. This is due to the fact that

the ballistic wave is only sensitive to the average scattering properties over the Fresnel zone [15][19]. The fact that the stability of the ballistic wave depends on perturbations with a length-scale that depends on the width of the Fresnel rather than a wavelength (as in the case for the coda waves) implies that fundamentally different mechanisms are relevant for the coda wave and the ballistic wave.

This study implies that waves and particles react in fundamentally different ways to perturbations of the initial conditions or the medium. The reason for this is that particles "select" a certain trajectory whereas waves travel along all possible trajectories visiting all the scatterers in all possible combinations. It is the "selection process" of a particle trajectory that creates the fundamentally larger instability of particle propagation than of wave propagation.

Note that a crucial element in the reasoning is the splitting of a wave when it meets a scatterer and is scattered in all directions. This suggests that ray splitting [14][20] is a crucial element for explaining the difference in the stability of the temporal evolution of waves and particles. This also applies to the quantum behavior of the periodically kicked rotator [6] because as shown in Fig. 1 of Casati[21] a localized wave packet in the quantum rotator rapidly breaks up.

The work presented here has implications for the relation between classical chaos and quantum chaos. The issue of the stability of wave propagation is also of interest in imaging problems [11] as well as for wave propagation problems in ocean acoustics [22][23] and seismology [24].

Corresponding author: R. Snieder

References

[1] M. Tabor, *Chaos and integrability in nonlinear dynamics* (Wiley and Sons, New York, 1989).

[2] Berry, M.V., *Proc. R. Soc. London,* **A356**, 183 (1987).

[3] Radons, G., J. Geisel and J. Rubner, *Adv. Chem. Phys.*, **73**, 891 (1989).

[4] Aleiner, I.L. and A.I. Larkin, *Chaos, Solitons and Fractals*, **8**, 1179 (1997).

[5] Gutzwiller, M.C., *Chaos in classical and quantum mechanics* (Springer-Verlag, New York, 1990).

[6] Ballentine, L.E. and J.P. Zibin, *Phys. Rev. A*, **54**, 3813 (1996).

[7] M. Derode, P. Roux and M. Fink, *Phys. Rev. Lett.,* **75,** 4206 (1995).

[8] Fink, M., *Phys. Today*, **50,** 34 (1997).

[9] Draeger, C. and M. Fink, *Phys. Rev. A*, **56**, 1767 (1997).

[10] L. Bunimovich, *Comm. Math. Phys.*, **65**, 295 (1979).

[11] J.A. Scales and R. Snieder, *Geophysics*, **62**, 1045 (1997).

[12] Brack, M. and R.K. Bhaduri, *Semiclassical physics* (Addison-Wesley, Reading MA, 1997).

[13] Zhao, L. and F.A. Dahlen, *Geophys. J. Int,* **115**, 729 (1993).

[14] Blümel, R., T.M. Antonsen, B. Georgeot, E. Ott and R.E. Prange, *Phys. Rev. Lett.*, **76**, 2476 (1996).

[15] Groenenboom J. and R. Snieder, *J. Acoust. Soc. Am.,* **98,** 3482 (1995).

[16] van de Hulst, H.C., *Physica*, **15**, 740 (1949).

[17] Ishimaru, I., *Wave propagation and scattering in random media* (Oxford Univ. Press, Oxford, 1997).

[18] Moret-Bailly, J., *Quantum Semiclass. Opt.*, **10**, L35 (1998).

[19] Snieder, R. and A. Lomax, *Geophys. J. Int.*, **125**, 796 (1996).

[20] Sirko, L., P.M. Koch and R. Blümel, *Phys. Rev. Lett.*, **78**, 2940 (1997).

[21] Casati, G., *Chaos*, **6**, 391 (1996).

[22] Tappert, F.D. and X. Tang, *J. Acoust. Soc. Am.*, **99**, 185 (1996).

[23] Wiercigroch, M., A.H.D. Cheng and J. Simmen, *Chaos, Solitons and Fractals*, **9**, 193 (1998).

[24] Keers, H., F.A. Dahlen and G. Nolet, *Geophys. J. Int.*, **131**, 361 (1997).

A The variance in the path length for the ballistic wave

For small scattering angles Θ_j the variance in the path length given in (20) reduces to

$$\sigma_L^2 = \sum_{j=1}^{n} \left\langle \Theta_j^2 \right\rangle \delta^2 \, . \tag{25}$$

As a model for the ballistic wave we assume the that n scatterers are separated with the same spacing Δ along the source-receiver path, this separation is given by

$$\Delta = \frac{L}{(n+1)} \, , \tag{26}$$

see Fig. 9. The fixed positions of the source and receiver are denoted by (x_0, z_0) and (x_{n+1}, z_{n+1}) respectively, hence $x_0 = x_{n+1} = 0$. The positions of the scatterers are prescribed by the distance x_j from the source-receiver line, the angle between the path from scatterer j to scatterer $j+1$ is denoted by φ_j. Since this angle is small $\varphi_j = (x_{j+1} - x_j)/\Delta$, so that

$$\Theta_j = \varphi_j - \varphi_{j-1} = (x_{j+1} - 2x_j + x_{j-1})/\Delta \, . \tag{27}$$

The variance in the path length follows by inserting (27) in (25). The cross terms that appear vanish on average because the positions of the scatterers are independent: $\langle x_{j+1} x_j \rangle = 0$. When all the scatterers have the same rms distance $\langle x^2 \rangle$ to the source-receiver line (with the exception of the terms $j = 0$ and $j = n+1$ for which $x_0 = x_{n+1} = 0$) it follows that $\sigma_L^2 = (6n-2) \langle x^2 \rangle \delta^2 / \Delta$. Given the crudeness of the scattering model, the factor -2 in this expression is ignored so that the scattering angle is approximately equal to

$$\sigma_L^2 = \frac{6\delta^2}{\Delta^2} n \left\langle x^2 \right\rangle \tag{28}$$

The rms distance $\langle x^2 \rangle$ is at this point unknown, this quantity follows from the requirement that the scatterers are located within the first Fresnel zone. The length L_j of the path from scatterer j to scatterer $j+1$ is given by $L_j = \sqrt{\Delta^2 + (x_{j+1} - x_j)^2} \approx \Delta + (x_{j+1} - x_j)^2 / 2\Delta$. The detour d of the scattered wave compared to the direct wave is thus given by:

$$d = \sum_{j=0}^{n} L_j - L = \frac{1}{2\Delta} \sum_{j=0}^{n} (x_{j+1} - x_j)^2 \tag{29}$$

Using the fact that the scatterer positions are uncorrelated one finds using $x_0 = x_{n+1} = 0$ that on average

$$\langle d \rangle = \frac{n \left\langle x^2 \right\rangle}{\Delta} \ . \tag{30}$$

The scatterers contribute to the ballistic wave when the detour is less than a quarter wavelength. Assuming that this corresponds to a mean detour $\langle d \rangle$ of $\lambda/8$ one finds the corresponding variance $\left\langle x^2 \right\rangle$ from (30):

$$n \left\langle x^2 \right\rangle = \frac{\lambda \Delta}{8} \ . \tag{31}$$

Using this in (28) and using (26) to eliminate Δ then gives the variance of the path length of the ballistic wave:

$$\sigma_L^{ball} = \sqrt{\frac{3(n+1)}{4}} \sqrt{\frac{\lambda}{L}} \, \delta \ . \tag{32}$$

Symbol	**Property**	**Value**
σ	Scattering cross section	1.592 mm
l	Mean free path	15.56 mm
λ	Dominant wavelength	2.5 mm

Table 1: Numerical values of parameters in numerical experiment.

n	$\delta_c(mm)$
1	0.0129
2	2.11×10^{-4}
3	3.43×10^{-6}
4	5.60×10^{-8}
5	9.11×10^{-10}
6	1.48×10^{-11}
7	2.41×10^{-13}
8	3.93×10^{-15}
Machine precision	0.22×10^{-15}
9	6.41×10^{-17}

Table 2: Critical error defined in equation (15) for different number of scattering encounters. Also indicated is the employed machine precision.

	Scatterer location	**Source location**
Particles	$\frac{1}{2}\left(\frac{\left(\frac{2\pi l}{\sigma}\right)-1}{\left(\frac{2\pi l}{\sigma}\right)^{n+1}-1}\right)\sigma$	$\frac{1}{2}\left(\frac{\sigma}{2\pi l}\right)^{n}\sigma$
Ballistic wave	$\frac{\sqrt{\lambda L}}{\sqrt{12(n+1)}}$	$\frac{\lambda}{4}$
Coda wave	$\frac{1}{\sqrt{2n}}\frac{\lambda}{4}$	$\frac{\lambda}{4}$

Table 3: Critical length scales δ_c for different perturbations.

Wave	**Time window (ms)**	**Number of encounters**
Ballistic	0.11-0.13	2
Coda 1	0.20-0.25	13
Coda 2	0.30-0.35	22
Coda 3	0.40-0.45	32

Table 4: Time windows used in the different numerical experiments with waves and number of scattering encounters.

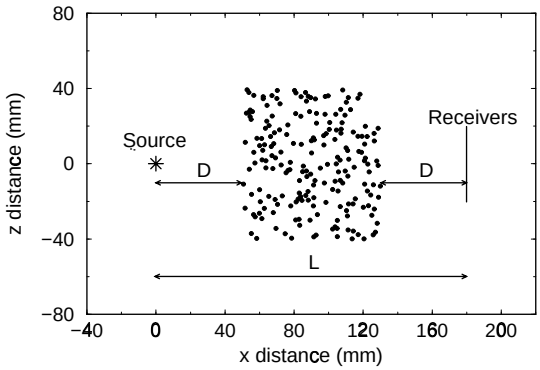

Figure 1: Geometry of the numerical experiment.

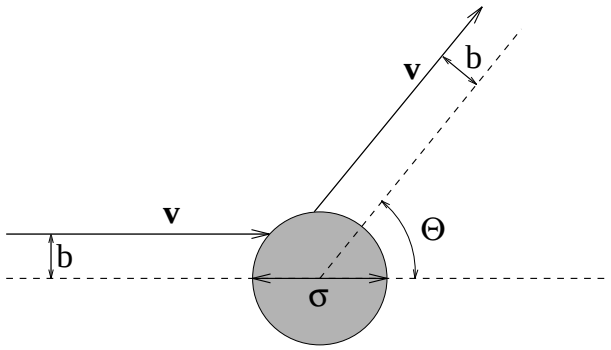

Figure 2: Definition of the impact parameter b.

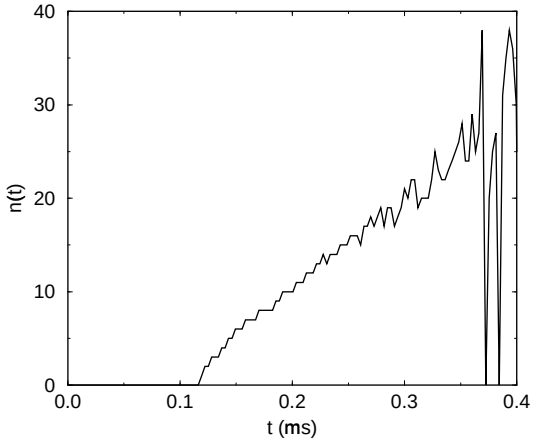

Figure 3: Mean number of scatterers encountered by particles as a function of arrival time at the receiver line.

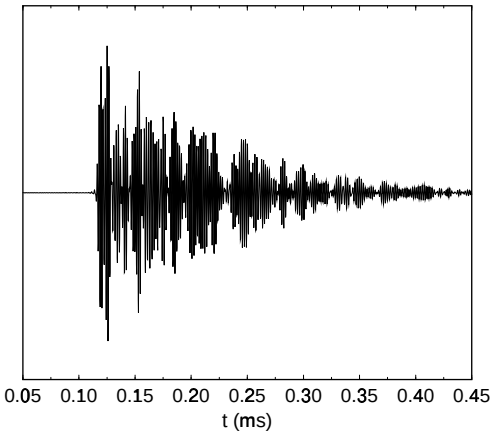

Figure 4: Wave field recorded at a receiver in the middle of the receiver line shown in Fig. 1.

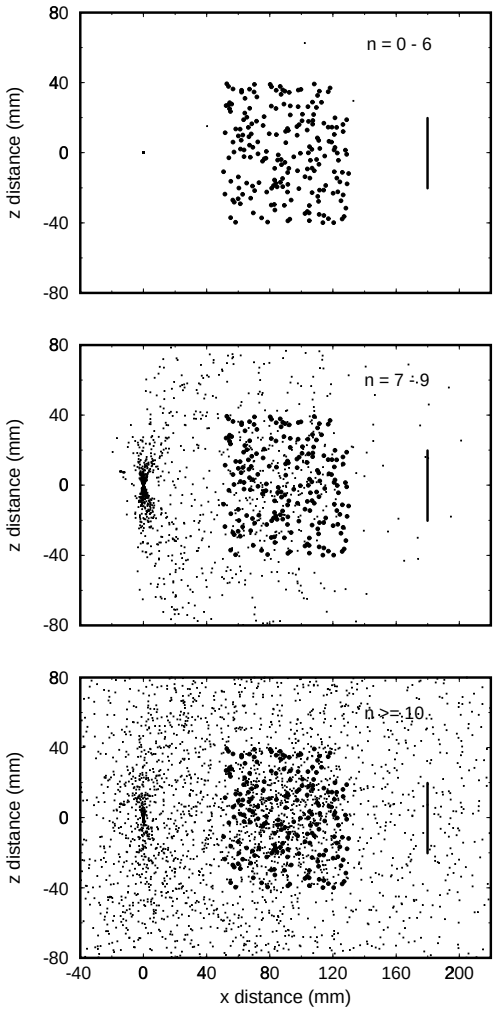

Figure 5: Location of particles at time $t = 0$ after TRI for (i) 6 or fewer scattering encounters (top panel), (ii) between 7 and 9 scattering encounters (middle panel) and (iii) more than 10 scattering encounters (bottom panel) as a function of the position of the x and z coordinates. Particles are indicated by thin dots, scatterers by large dots.

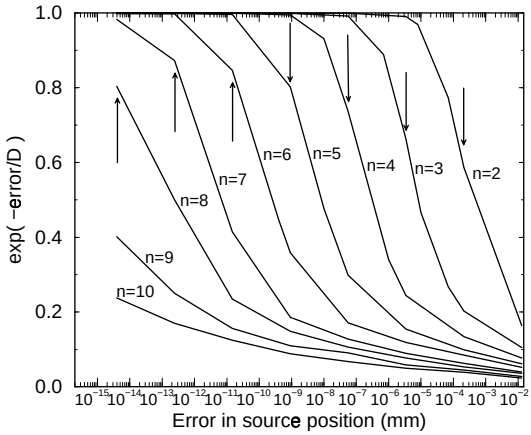

Figure 6: Imaging quality defined as $exp(-error/D)$ as a function of the perturbation in the initial position of the time reversal of particles. Estimates of the critical perturbation defined in equation (15) are indicated by vertical arrows.

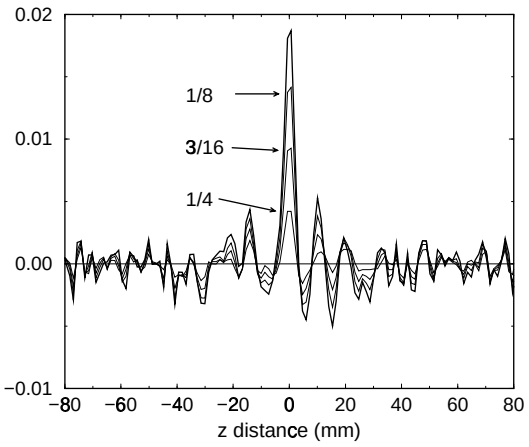

Figure 7: Time reversed wave-field at time $t = 0$ along the line $x = constant$ through the source. The source location is at location $z = 0$. The thick solid lines are for the unperturbed receiver positions. The thin solid lines are for the TRI wave-field with perturbed receiver positions. The numbers denote the rms value of the perturbation as a fraction of the dominant wavelength.

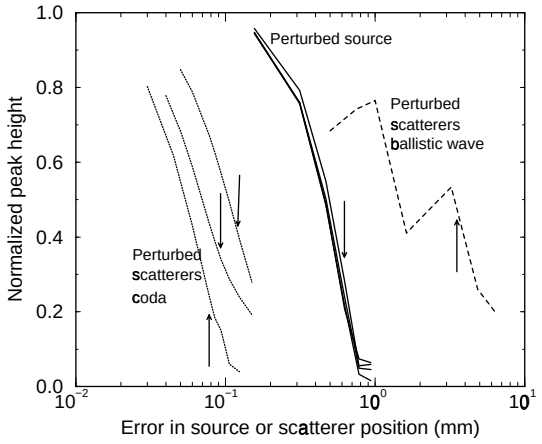

Figure 8: Quality of TRI of waves measured as ratio of the peak height of the imaged section for the experiment with perturbed conditions compared to the TRI experiment without perturbations as a function of the perturbation in source or scatterer position. The dashed line represents the ballistic waves with perturbed scatterers. The dotted lines on the left are for the coda intervals shown in Table (4) for perturbed scatterers with the latest coda interval in the left. The solid lines are for a perturbed source position for the ballistic wave and the three coda intervals. The critical length scales from Table (3) are shown by vertical arrows.

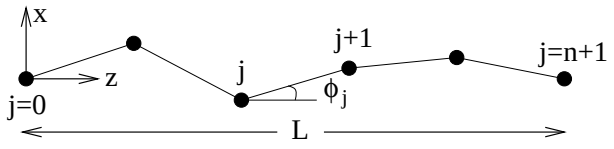

Figure 9: Definition of the geometric variables used for the calculation of the variance of the path length of the ballistic wave.